$RbEu(Fe_{1-x}Ni_x)_4As_4$: From a ferromagnetic superconductor to a superconducting ferromagnet

Yi Liu,[1] Ya-Bin Liu,[1] Ya-Long Yu,[1] Qian Tao,[1] Chun-Mu Feng,[1] and Guang-Han Cao[1,2,3,*]

[1]*Department of Physics, Zhejiang University, Hangzhou 310027, China*

[2]*State Key Lab of Silicon Materials, Zhejiang University, Hangzhou 310027, China*

[3]*Collaborative Innovation Centre of Advanced Microstructures, Nanjing 210093, China*

(Received 18 September 2017; revised manuscript received 29 November 2017; published 22 December 2017)

The intrinsically hole-doped $RbEuFe_4As_4$ exhibits bulk superconductivity at $T_{sc} = 36.5$ K and ferromagnetic ordering in the Eu sublattice at $T_m = 15$ K. Here we present a hole-compensation study by introducing extra itinerant electrons via a Ni substitution in the ferromagnetic superconductor $RbEuFe_4As_4$ with $T_{sc} > T_m$. With the Ni doping, T_{sc} decreases rapidly, and the Eu-spin ferromagnetism and its T_m remain unchanged. Consequently, the system $RbEu(Fe_{1-x}Ni_x)_4As_4$ transforms into a superconducting ferromagnet with $T_m > T_{sc}$ for $0.07 \leqslant x \leqslant 0.08$. The occurrence of superconducting ferromagnets is attributed to the decoupling between Eu^{2+} spins and superconducting Cooper pairs. The superconducting and magnetic phase diagram is established, which additionally includes a recovered yet suppressed spin-density-wave state.

DOI: 10.1103/PhysRevB.96.224510

I. INTRODUCTION

Superconductivity (SC) and ferromagnetism (FM) are basically antagonistic and incompatible [1,2], and only in a very few cases can they coexist simultaneously in a single material [1,3]. The relative robustness of SC and FM can be reflected by the superconducting critical temperature T_{sc} and the (ferro)magnetic transition temperature T_m. Materials with $T_{sc} > T_m$ were earlier called "ferromagnetic superconductors" (FSCs) [1], and those with $T_m > T_{sc}$ were then termed "superconducting ferromagnets" (SFMs) [4–6]. Generally, a ferromagnetic exchange field prevails over the intrinsic superconducting upper critical field H_{c2}^* for $T_m \leqslant T_{sc}$, hence SFMs are particularly rare. So far, examples of SFMs only include U-based germanides with spin-triplet SC [7] and ruthenocuprates with spin-singlet high-temperature SC [8], the second of which actually exhibits the coexistence with a canted antiferromagnetism. Note that the classification into FSCs and SFMs is meaningful for studying the way of coexistence of the two antagonistic phenomena [5,9].

In recent years, Eu-containing 122-type iron arsenides have earned a lot of interest owing to the intriguing interplay between SC and FM [3,10]. The crystal structure allows the magnetic Eu-atomic planes away from the superconductively active Fe-atom sheets. In nondoped $EuFe_2As_2$, the Eu sublattice is of an *A*-type antiferromagnetism below ~19 K while the Fe sublattice exhibits a spin-density-wave (SDW) order below ~190 K [11–14]. SC at $T_{sc} = 20$–30 K can be induced by the chemical doping with P [15], Co [16], Ru [17], Ir [18,19], and so on. Simultaneously, the Eu^{2+} local spins become *ferromagnetically* ordered at $T_m \sim 18$ K [20–24]. It has been concluded that SC appears only when $T_{sc} > T_m$ in systems of $EuFe_2(As_{1-x}P_x)_2$ [25,26], $Eu(Fe_{1-x}Co_x)_2As_2$ [27], and $Sr_{1-y}Eu_y(Fe_{0.88}Co_{0.12})_2As_2$ [28]. The conclusion also fits with the absence of SC in $Eu(Fe_{1-x}Ni_x)_2As_2$ [29] since the Eu-free analogous system $Sr(Fe_{1-x}Ni_x)_2As_2$ shows a maximum T_{sc} of 9.8 K, which is significantly lower than the expected T_m [30].

Very recently, a variant of $EuFe_2As_2$, i.e., the 1144-type $AEuFe_4As_4$ (A = Rb and Cs), were synthesized and characterized [31–33]. The twin compounds adopt a crystal structure identical to that previously designed [34], which was first realized in $AeAFe_4As_4$ (Ae = Ca, Sr; A = K, Rb, Cs) [35]. In $RbEuFe_4As_4$, the Rb^+ and Eu^{2+} planes, sandwiched by FeAs layers, stack alternately along the *c* axis. The structure can also be viewed as an intergrowth between nondoped $EuFe_2As_2$ and heavily overdoped $RbFe_2As_2$. As a result, $RbEuFe_4As_4$ is intrinsically hole-doped, exhibiting SC at $T_{sc} = 36.5$ K without any SDW ordering [31,32]. Additionally, evidence of FM of the Eu^{2+} spins below $T_m = 15$ K is given by magnetization measurements [32]. Compared to 122-type FSCs, the T_{sc} value is significantly higher, and the T_m value is slightly lower. Important to be noted is that the T_{sc} value of $RbEuFe_4As_4$ is almost the same as, or even larger than, those of the nonmagnetic analogues (e.g., $T_{sc} = 35.1$ K in $RbSrFe_4As_4$ [35]), indicating that the Eu^{2+} spins hardly break superconducting Cooper pairs. In this context, SC may survive easily in the presence of Eu-spin order, and therefore, it is of interest to seek for an SFM in the 1144-type system.

Now that $RbEuFe_4As_4$ bears an intrinsic hole doping (0.25 holes per Fe atom), it is natural to tune the T_{sc} value by hole depletion via electron doping. Our preliminary trial with a Ba-for-Rb substitution was demonstrated unsuccessful since a 122-type phase, instead of the expected 1144-type phase, became stabilized. Then, we turned to a substitution at the Fe site. To compensate the doped holes more effectively, we chose Ni as the dopant because Ni^{2+} ($3d^8$) has two more itinerant electrons than Fe^{2+} ($3d^6$) does, and more importantly, previous Ni-doping studies indeed showed such an effect of electron doping [30,36,37].

In this paper, we report a systematic investigation on the magnetic and superconducting properties in $RbEu(Fe_{1-x}Ni_x)_4As_4$. As expected, T_{sc} decreases rapidly with the Ni doping. On the other hand, the Eu-spin FM and its T_m value remain unchanged. This leads to a discovery of SFMs in $RbEu(Fe_{1-x}Ni_x)_4As_4$ with $0.07 \leqslant x \leqslant 0.08$, in which SC survives when T_{sc} becomes lower than T_m. The SFMs are found to show no Meissner state with a broadened resistive transition

*ghcao@zju.edu.cn

because they are always under the internal field generated by the FM of Eu^{2+} spins. The superconducting and magnetic phase diagram has been established, and the reason for the existence of SFMs is discussed.

II. EXPERIMENTAL METHODS

Polycrystalline samples of $RbEu(Fe_{1-x}Ni_x)_4As_4$ with $0 \leqslant x \leqslant 0.125$ were prepared by solid-state reactions in evacuated quartz ampoules sealed, similar to our previous report [32]. The source materials were the constituent elements: Rb (99.75%), As (99.999%), Eu (99.9%), Fe (99.998%), and Ni (99.99%), all from Alfa Aesar. First, precursors of EuAs, FeAs, NiAs, and $RbFe_2As_2$ (with 5% excess of Rb) were prepared by solid-state reactions in evacuated quartz tubes at 873 to 1023 K for 24 hours. These precursors and additional Fe powders were then mixed together in the nominal composition of $RbEu(Fe_{1-x}Ni_x)_4As_4$, followed by thoroughly homogenizing with ball milling in an Ar-filled glove box. Second, the mixtures were pressed into pellets which were loaded in an alumina container jacketed with a double-layer protector (a sealed Ta tube inside and a quartz ampoule outside). Finally, the samples were rapidly heated to 1133 K, holding for 20 hours, ended with quenching in cool water. To improve the samples' purity, the synthesis was repeated once or twice, with an intermediate grinding.

Powder x-ray diffraction (XRD) was performed on a PANalytical x-ray diffractometer with a monochromatic Cu-$K_{\alpha 1}$ radiation at room temperature. The lattice parameters were obtained by a least-squares fit of 15 to 25 reflections in the range of $5^\circ \leqslant 2\theta \leqslant 80^\circ$. The sample's chemical composition was checked by energy-dispersive x-ray spectroscopy (EDS). The resistivity and specific-heat measurements were conducted on a Quantum Design Physical Property Measurement System (PPMS-9). The dc magnetization was measured on a Quantum Design Magnetic Property Measurement System (MPMS-XL5).

III. RESULTS AND DISCUSSION

A. X-ray diffraction

Figure 1(a) shows XRD patterns of the series samples of $RbEu(Fe_{1-x}Ni_x)_4As_4$ ($0 \leqslant x \leqslant 0.1$), which can be well indexed by a tetragonal unit cell with $a \approx 3.89$ Å and $c \approx 13.3$ Å. The variations in relative intensity are mainly due to (00l) preferred orientations. One sees that all the samples from $x = 0$ to 0.1 are nearly single phase (only a small amount of impurities such as FeAs appear in some of the samples). In the case of $x = 0.125$, the XRD pattern (not shown) indicates the formation of 122-type phase. Therefore, the present study is limited to samples with $0 \leqslant x \leqslant 0.1$.

The lattice constants were determined by a least-squares fit, the results of which are displayed in Table I. Figures 1(b) and 1(c) plot the fitted lattice parameters a and c, respectively, as a function of the nominal Ni content. As is shown, while the a axis of the unit cell basically remains unchanged, the c axis decreases significantly with the Ni doping. The result is quite similar to those in $Eu(Fe_{1-x}Ni_x)_2As_2$ [29], $LaFe_{1-x}Ni_xAsO$ [36], and $Ba(Fe_{1-x}Ni_x)_2As_2$ [37] systems. The linear decrease in c, which obeys the Vegard's law,

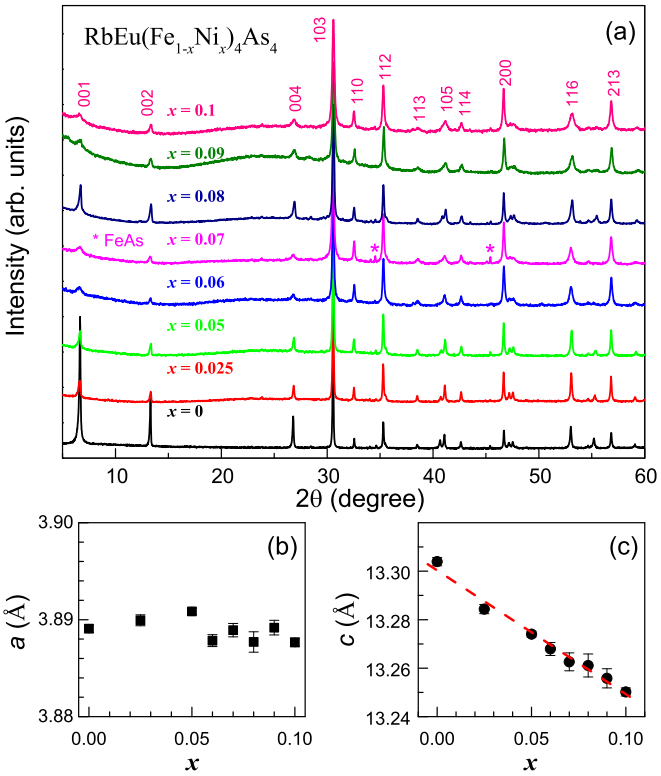

FIG. 1. (a) Powder x-ray diffraction patterns of $RbEu(Fe_{1-x}Ni_x)_4As_4$ ($0 \leqslant x \leqslant 0.1$) at room temperature. (b, c) Lattice parameters a and c as functions of the nominal Ni concentration x. The dashed line in (c) gives the linear fit.

confirms that the dopant Ni indeed substitutes for Fe. The EDS on the sample of $x = 0.1$ shows that the Ni content is 0.089(8), which remains unchanged throughout the sample. This confirms that the sample is homogeneous for the Ni doping, and the actual Ni-doping level is close to the nominal one within the measurement uncertainty.

B. Magnetic properties

We first address the Eu-spin state by focusing on the high-temperature magnetic properties in $RbEu(Fe_{1-x}Ni_x)_4As_4$. As is shown in Fig. 2, the magnetic susceptibility (χ) at high temperatures is of Curie-Weiss-type paramagnetism. The $\chi(T)$ data in the temperature range of $50\ \mathrm{K} \leqslant T \leqslant 300\ \mathrm{K}$ can be well fitted with an extended Curie-Weiss law $\chi = \chi_0 + C/(T - \Theta)$, where χ_0 is the temperature-independent term, C gives the Curie constant from which the effective local moment is derived, and Θ represents the Curie-Weiss temperature. The derived effective moment μ_{eff} (see Table I) ranges between 7.46 and 8.00 μ_B/f.u. (f.u. refers to formula unit), independent of the Ni substitution. These μ_{eff} values are close to that (7.9 μ_B) expected for a free Eu^{2+} ion, indicating a spin state with total spins of $S = 7/2$ for the Eu^{2+} ions. The Θ values fitted (from 23.6 to 24.8 K) is also independent of the Ni doping. The positive sign of Θ reflects dominant ferromagnetic interactions between Eu^{2+} spins.

At low temperatures, the system undergoes superconducting and/or magnetic transitions. To determine their transition temperatures, T_{sc} and T_{m}, we performed the measurement

TABLE I. Room-temperature lattice constants and physical-property parameters of RbEu(Fe$_{1-x}$Ni$_x$)$_4$As$_4$ ($0 \leqslant x \leqslant 0.1$). The digits in parentheses give two times the standard deviation of the least-squares fit. T_{sc}^{ρ} is the superconducting midpoint transition temperature in the resistivity measurement. T_{SDW} denotes the spin-density-wave transition temperature. T_m and Θ are the magnetic-transition and Curie-Weiss temperatures, respectively. μ_{eff} and M_{sat} are the effective magnetic moment in the paramagnetic state and the ordered moment in the ferromagnetic state, respectively. H_{coe} refers to the apparent coercive field.

	Lattice Constants		Physical-Property Parameters						
x	a(Å)	c (Å)	T_{sc}^{ρ} (K)	T_{SDW} (K)	T_m (K)	Θ (K)	μ_{eff} (μ_B/Eu)	M_{sat} (μ_B/Eu)	H_{coe} (Oe)
0	3.8891(4)	13.304(17)	36.4	–	15.0	23.6	7.95	6.5	360
0.025	3.8900(6)	13.284(19)	30.3	–	15.0	24.3	7.88	6.5	258
0.05	3.8909(3)	13.274(12)	23.0	28.9	15.0	24.5	8.00	6.4	88
0.06	3.8878(6)	13.268(27)	18.1	31.1	15.0	24.3	7.65	5.9	67
0.07	3.8889(7)	13.263(37)	11.2	35.0	15.1	24.2	7.46	5.9	44
0.08	3.8877(11)	13.261(48)	2.1	33.6	14.7	24.4	7.85	6.5	21
0.09	3.8892(8)	13.256(40)	–	31.3	14.7	24.8	7.79	6.0	20
0.1	3.8877(4)	13.250(17)	–	29.4	14.8	24.4	7.74	6.3	24

of temperature-dependent magnetization, $M(T)$, under a low field of 10 Oe. In general, a superconducting transition can be easily recognized by the strong diamagnetic signal owing to the Meissner effect. However, in cases of the coexistence between SC and FM with $T_{sc} \leqslant T_m$, the diamagnetic signal may be covered up by FM. For the ferromagnetic transition, on the other hand, the Curie temperature is traditionally determined by the Arrot approach [38]. However, the presence of SC makes the method invalid. Here we take advantage of the magnetic hysteresis arising from the appearance of magnetic domains. Namely, T_m is defined by the bifurcation temperature between field-cooling (FC) and zero-field-cooling (ZFC) $M(T)$ data measured under magnetic fields lower than the coercive field. In fact, the bifurcation point basically coincides with the kink (peak) in the FC (ZFC) curves.

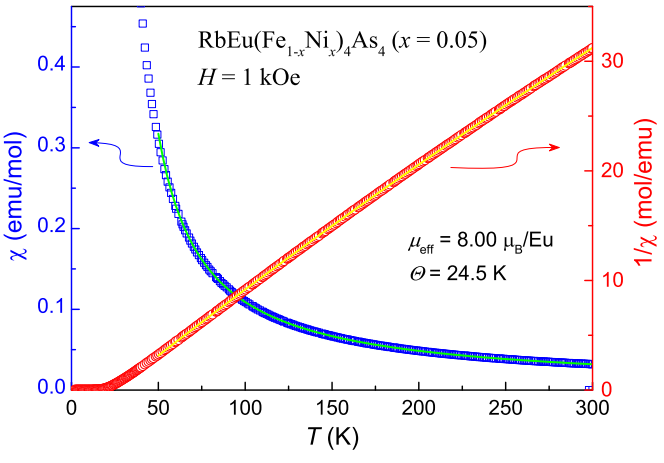

FIG. 2. Temperature dependence of dc magnetic susceptibility ($\chi = M/H$) for a typical sample of RbEu(Fe$_{1-x}$Ni$_x$)$_4$As$_4$ with $x = 0.05$ at a magnetic field of $H = 1$ kOe. The right-hand axis plots $1/\chi$, indicating dominant Curie-Weiss paramagnetism above 25 K. The data in the range of 50 K $\leqslant T \leqslant$ 300 K are fitted with Curie-Weiss law (displayed with solid lines), from which the effective local moment μ_{eff} and the Curie-Weiss temperature Θ are extracted as shown. See the text for details.

Furthermore, the resultant T_m value is precisely consistent with the heat-capacity measurement [32]. Note that a type-II SC may also give rise to a bifurcation between FC and ZFC curves owing to the magnetic flux-pinning effect.

Figures 3(a) to 3(h) shows the low-field $M(T)$ data for samples of the RbEu(Fe$_{1-x}$Ni$_x$)$_4$As$_4$ series. The nondoped ($x = 0$) compound shows SC at $T_{sc} = 36.5$ K and FM below $T_m = 15$ K [32]. For $x = 0.025$, the superconducting transition keeps robust, yet with an obviously reduced T_{sc} of 30.5 K. At $x = 0.05$, in which T_{sc} is further decreased to 22 K, the superconducting transition becomes much less remarkable. For $x = 0.06$, only the weak signature of SC at 15.7 K can be traced from the slight difference between the FC and ZFC data, the second of which comes from the flux-pinning effect. The existence of SC is also evidenced from the diamagnetism in the ZFC data at lower temperatures and, in particular, from the zero resistance at 16 K in the resistivity measurement shown below. In the cases of $x \geqslant 0.07$, no magnetic signal for SC can be detected, although the resistivity measurement clearly shows superconducting transitions at lower temperatures for $0.07 \leqslant x \leqslant 0.08$.

In contrast to the monotonic suppression in T_{sc} with increasing Ni doping, the magnetic transition temperature T_m almost remains unchanged. Note that the Curie-Weiss temperature Θ, which is remarkably higher than T_m, does not depend on the Ni doping either. The lower-than-expected T_m value is probably related to the quasi-two-dimensional magnetism caused by a much weaker magnetic coupling along the c axis [32]. We will discuss the magnetic interactions later on.

One may also note that, for lower Ni doping with $x \leqslant 0.05$, the FC magnetization *decreases* with decreasing temperature just below T_m, showing a peak-like anomaly (PLA) at T_m, which casts doubt on the nature of the magnetic transition. To address this issue, we measured the $M(T)$ data at elevated magnetic fields shown in Fig. 4. One sees that the PLA disappears under relatively low fields (~0.5 kOe). At higher fields with $H \geqslant 5$ kOe, all the $M(T)$ curves become almost identical without bifurcations in the FC and ZFC data, suggesting commonality of FM in the system. In fact, a similar PLA behavior is also seen in 122-type FSCs [16,39] where an

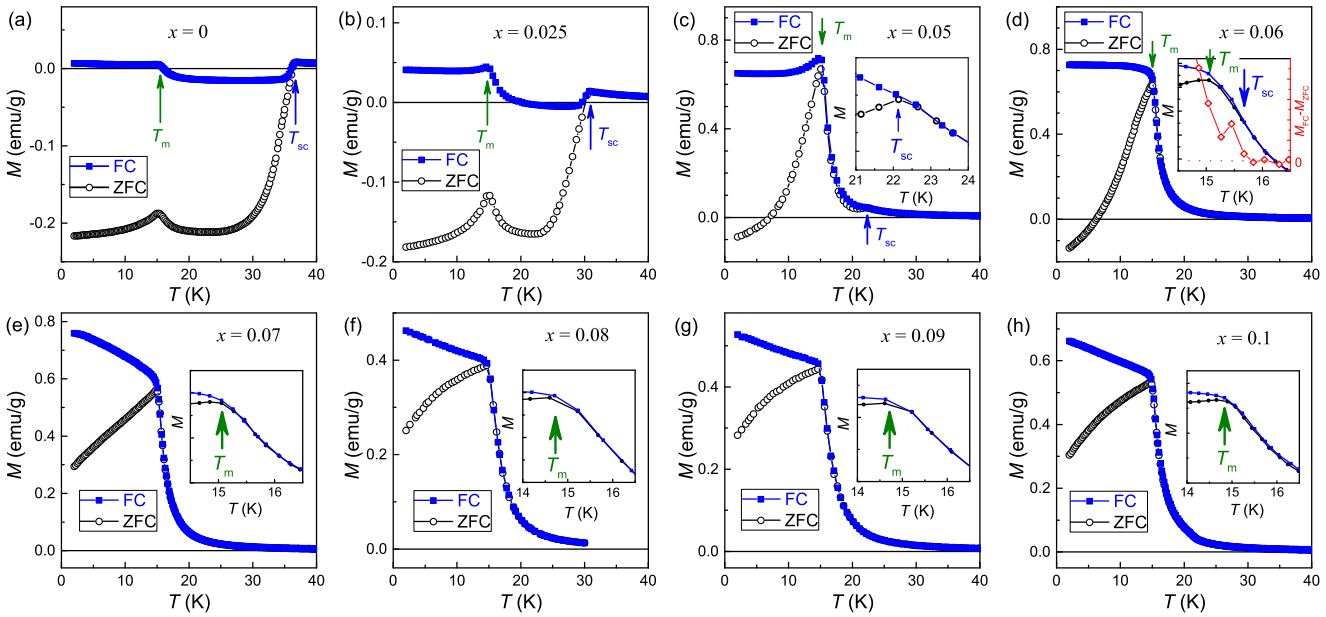

FIG. 3. Temperature dependence of magnetization under a magnetic field of 10 Oe for $RbEu(Fe_{1-x}Ni_x)_4As_4$ ($0 \leqslant x \leqslant 0.1$) samples. FC (solid symbols) and ZFC (open symbols) denote field cooling and zero-field cooling, respectively, in the magnetic measurements. T_{sc} and T_m marked with arrows represent the superconducting and magnetic transition temperatures, respectively. The insets show close-ups near the superconducting/magnetic transitions. The inset in panel (d) also plots the difference between the FC and ZFC data, using the righ-hand axis.

Eu-spin FM is unambiguously demonstrated [20–22]. Note that the PLA here happens only for $T_{sc} > T_m$. This suggests that the PLA is probably in relation to the presence of SC. As is pointed out theoretically, the state of FM may be modified into cryptoferromagnetism [40] or dense-domain structure [41] owing to the presence of SC. The expected fine ferromagnetic domains that are antiferromagnetically aligned could give rise to a PLA in the FC $M(T)$ curve. Future studies with single-crystalline samples by magnetic-force microscopy [42] seem promising to clarify this issue.

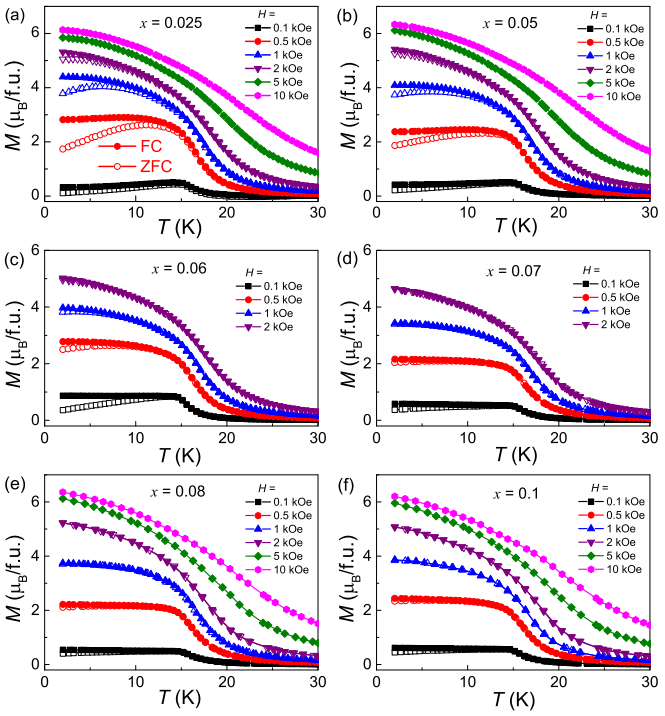

FIG. 4. Temperature dependence of field-cooling (FC, solid symbols) and zero-field-cooling (ZFC, open symbols) magnetization under different magnetic fields for (a) $x = 0.025$, (b) 0.05, (c) 0.06, (d) 0.07, (e) 0.08, and (f) 0.1 in $RbEu(Fe_{1-x}Ni_x)_4As_4$. The magnetization is conversed into Bohr magnetons per formula unit.

The Eu-spin FM in $RbEu(Fe_{1-x}Ni_x)_4As_4$ is further confirmed by the isothermal magnetization, $M(H)$, shown in Figs. 5(a) to 5(f). At high temperatures (e.g., 40 K), the $M(H)$ data are essentially linear, consistent with the paramagnetic state of Eu^{2+} spins. At temperatures below T_m, by contrast, the $M(H)$ curves are of an S shape, characteristic of an FM. The saturation magnetization M_{sat}, defined here as the magnetization value at 1 T and 2 K, scatters from 5.9 to 6.5 μ_B/f.u. (see Table I). Samples containing more FeAs impurity tend to have relatively low M_{sat} (and μ_{eff} also). Other samples show an M_{sat} value that is close to the expected one (7.0 μ_B per Eu^{2+}) [43], indicating that Eu^{2+} spins order ferromagnetically.

Note that for samples of $x \leqslant 0.05$, which have higher T_{sc} values, the magnetic hysteresis is extended to high fields where the magnetization is saturated. This clearly indicates the existence of type-II SC that commonly exhibits the flux-pinning effect, the latter of which also gives rise to an enhancement of the apparent coercive field H_{coe}. As is shown in Table I, the intrinsic H_{coe}, given by nonsuperconducting samples of $0.08 < x \leqslant 0.1$, is actually around 20 Oe. The sample of $x = 0.07$ shows an enhanced H_{coe} of 44 Oe, implying the existence of SC. Indeed, the resistivity measurement below demonstrates a superconducting transition at $T_{sc} = 11$ K, 4 K lower than T_m. That is to say, the sample is actually an SFM. Notably, no superconducting diamagnetism is detected by the $M(T)$ data [Fig. 3(e)] and the virgin $M(H)$ curve [Fig. 5(c)].

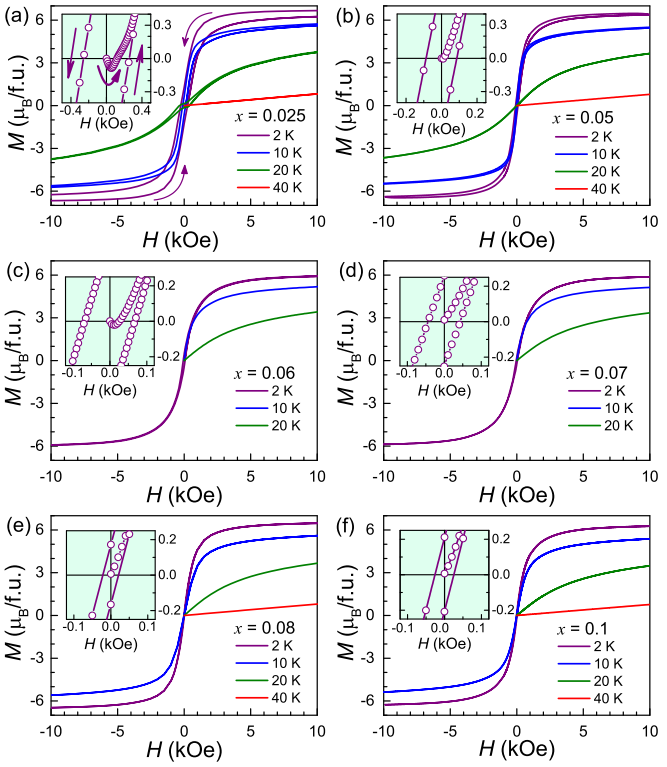

FIG. 5. Isothermal magnetization at low temperatures in the RbEu(Fe$_{1-x}$Ni$_x$)$_4$As$_4$ series. The insets show close-ups of the magnetic hysteresis at 2 K, from which the virgin magnetization as well as the coercive field can be seen clearly.

This observation is consistent with the absence of the Meissner state, as expected from the internal field (∼4.5 kOe [44]) that is much higher than the intrinsic lower critical field. It is of great interest for the future to look into the anisotropic magnetic properties with using the single-crystalline samples.

C. Electrical resistivity

Figure 6 shows the electrical resistivity (ρ) for RbEu(Fe$_{1-x}$Ni$_x$)$_4$As$_4$ polycrystalline samples. To highlight the evolution of the temperature dependence, and also to present the superconducting/SDW transitions clearly, we normalize the $\rho(T)$ data relative to the resistivity values at 200 and 50 K, respectively. First of all, the slope $d\rho/dT$ in the normal state decreases monotonically with the Ni doping, giving rise to an increase in the residual resistivity at low temperatures. This is consistent with the increase of Fe-site disorder with Ni doping. Second, the superconducting transition temperature T_{sc}^{ρ} decreases with the Ni doping, and SC is completely suppressed at $x = 0.09$ (the slight drop around 5 K is probably due to the sample's inhomogeneity). The result is basically consistent with the magnetic measurement for $x \geqslant 0.06$ with $T_{sc} > T_m$. In the case of $T_{sc} \leqslant T_m$, nevertheless, SC cannot be directly detected in the magnetic measurement above, and the resistive transitions become remarkably broadened. The broadened resistive transition is similar to the observation in Eu(Fe$_{0.81}$Co$_{0.19}$)$_2$As$_2$ [45] also with $T_{sc} < T_m$, which can be explained in terms of the dissipative flow of spontaneous vortices [9].

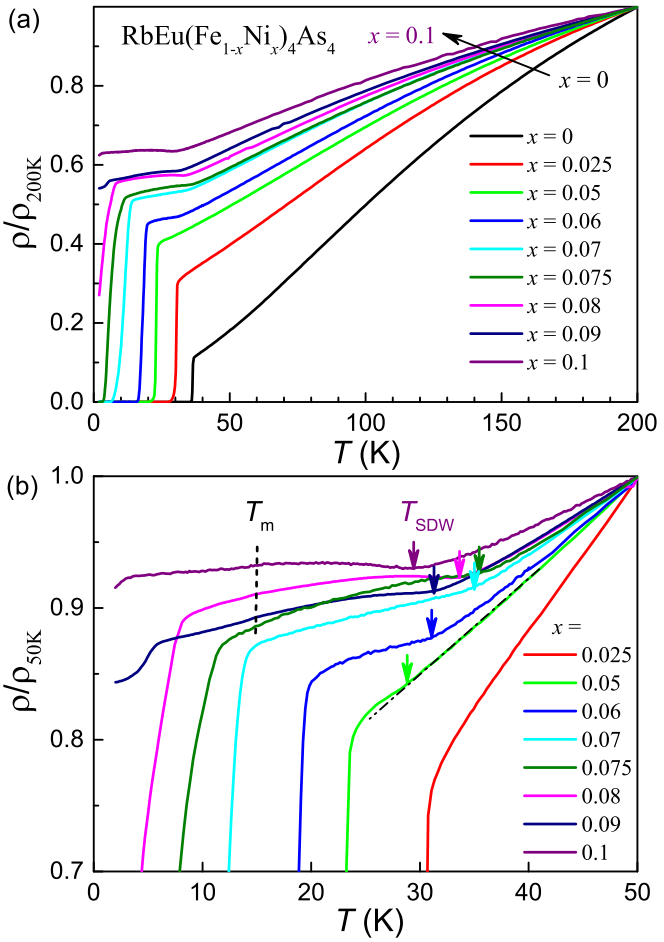

FIG. 6. Temperature dependence of resistivity for RbEu(Fe$_{1-x}$Ni$_x$)$_4$As$_4$ polycrystalline samples at zero field. The top and bottom panels adopt a normalized scale relative to the resistivity values at 200 and 50 K, respectively. In the bottom panel, the arrows labeled with T_{SDW} point to the resistivity upturn that probably comes from a spin-density-wave (SDW) transition. The left dashed line labeled with T_m marks the tiny kinks at which the Eu^{2+} spins order ferromagnetically.

Another interesting point is that the samples with $x \geqslant 0.05$ show a resistivity upturn above T_{sc}, which is probably due to a spin-density-wave (SDW) ordering in the Fe sublattice. At $x = 0.05$, the hole concentration is reduced to $n_h = 0.15$ holes per Fe atom, if assuming that every doped Ni atom depletes two holes. In the prototype Ba$_{1-x}$K$_x$Fe$_2$As$_2$ system, SDW order remains at $n_h = 0.15$ [46]. Note that the SDW transition temperature T_{SDW} here is much lower than expected. Furthermore, T_{SDW} decreases with x in the high doping regime. These results can be ascribed to the Fe-site disorder mentioned above. Similarly, a recovery of SDW by charge compensation was reported in Ba$_{1-x}$K$_x$Fe$_{1.86}$Co$_{0.14}$As$_2$ [47] and Eu$_{0.5}$K$_{0.5}$(Fe$_{1-x}$Ni$_x$)$_2$As$_2$ [48] systems. Here we note that, according to a recent report on Ni- and Co-doped CaKFe$_4$As$_4$ [49], the recovered SDW phase may have strikingly different magnetic order.

In addition to the SDW-like anomaly above, Fig. 6(b) also shows a very slight (yet observable) kink at T_m. This is due to the reduction of magnetic scattering on the charge carriers

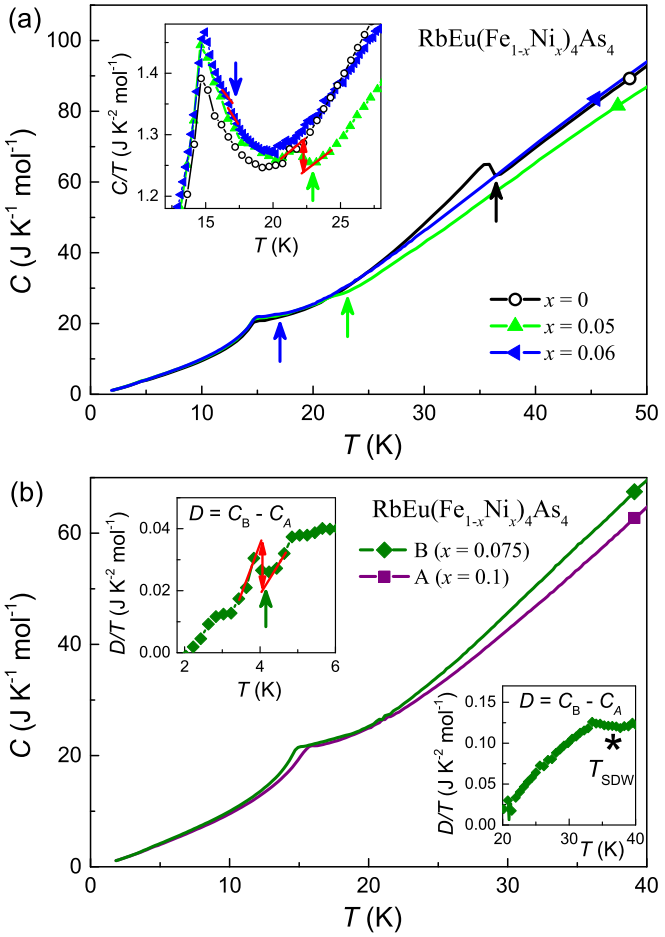

FIG. 7. Temperature dependence of specific heat capacity (C) of (a) the ferromagnetic superconductors and (b) the superconducting ferromagnet in $RbEu(Fe_{1-x}Ni_x)_4As_4$ under zero magnetic field. The superconducting transitions are marked by arrows. Note that the insets in the top and bottom panels plot C/T and D/T, respectively, where D stands for the specific-heat difference between samples of $x = 0.075$ and 0.1.

when Eu^{2+} spins become ordered, akin to the case in $EuFe_2As_2$ [11]. The tiny resistivity change at T_m seems to reflect weak interactions between Eu^{2+} spins and the charge carriers.

D. Heat capacity

Figure 7 shows the temperature dependence of the specific heat of $RbEu(Fe_{1-x}Ni_x)_4As_4$ under zero field, tracking for superconducting transitions in the FSCs and SFMs. For $x = 0$, the specific-heat jump is clearly seen with $\Delta C/T_{sc} = 208$ mJ K^{-2} mol^{-1} at the superconducting transition [32]. With increasing the Ni doping, the specific-heat jump becomes unapparent. At $x = 0.05$ and 0.06, for example, the $\Delta C/T_{sc}$ values are estimated to be ~50 and ~20 mJ K^{-2} mol^{-1}, respectively. A similar dramatic reduction in ΔC was also observed in underdoped $Ba_{1-x}K_xFe_2As_2$ [50]. As a comparison, the underdoped $Ba_{0.77}K_{0.23}Fe_2As_2$ sample ($T_{sc} = 23$ K) shows a $\Delta C/T_{sc}$ value of ~40 mJ K^{-2} mol^{-1} [50], comparable to that of the $x = 0.05$ sample (with a similar T_{sc}) in the present system. Note that the strength of superconducting coupling varies with the doping level [50], the former of which is reflected by the dimensionless parameter, $p = \Delta C/\gamma_n T_{sc}$, where γ_n denotes the Sommerfeld coefficient in the normal state. The drastic reduction in ΔC for the underdoped samples is actually a consequence of the *concurrent* decrease in all the three factors: γ_n, T_{sc}, and p.

In the case of SFMs with $T_{sc} < T_m$, no specific-heat anomaly at T_{sc} can be directly seen from the raw data. Nevertheless, by subtraction of the specific heat between the superconducting ($x = 0.075$) and nonsuperconducting ($x = 0.1$) samples, the specific-heat jump is still observable at 4.1 K (at which the resistivity drop to 6%), as shown in the upper-left inset of Fig. 7(b) (note that the kink at ~5 K is probably due to an antiferromagnetic transition from the very small amount of Eu_3O_4 impurity [51]). Since the Sommerfeld coefficient is greatly reduced in the underdoped regime [50], the $\Delta C/T_{sc}$ value (~10 mJ K^{-2} mol^{-1}) is actually appreciable, which supports the bulk nature of superconductivity. Additionally, from the specific-heat difference shown in the lower inset, one can see another anomaly at ~36 K (albeit no anomaly is observable again in the raw data), in accordance with the resistivity upturn. This anomaly, if being intrinsic, should be related to the recovered SDW transition.

E. Phase diagram

The results above allow us to construct the phase diagram in $RbEu(Fe_{1-x}Ni_x)_4As_4$, which is displayed in Fig. 8. As usual, the bottom axis employs the direct control parameter, i.e., the Ni content x. Since the substitution of Fe^{2+} ($3d^6$) with Ni^{2+} ($3d^8$) doubly compensates the self-doped holes, the expected hole concentration is $n_h = 0.25 - 2x$, which is also shown in the middle horizontal axis. With the hole depletion by Ni doping, T_{sc} decreases monotonically. Note that T_{sc} decreases more rapidly for $x \geqslant 0.05$ where SDW order appears, suggesting a competing nature between SC and SDW. SC disappears at $x > 0.08$ or at $n_h \leqslant 0.09$. One notes that T_{SDW} goes down for $x \geqslant 0.075$.

To understand the possible role of disorder, we compare to the electronic phase diagram of $Ba_{1-y}K_yFe_2As_2$ [52] which is disorder-free at the Fe site. One sees that the T_{sc} values in $RbEu(Fe_{1-x}Ni_x)_4As_4$ are overall lower in the doping area, and the critical hole concentration (for appearance of SC) is significantly higher. On the other hand, the T_{SDW} values are even much lower, especially in the high doping regime. Both results strongly suggest that the disorder by Ni doping plays an important role in suppressing SC as well as SDW.

Then, how much do the Eu^{2+} spins influence the T_{sc}? As we emphasize in the Introduction, first of all, SC in $RbEuFe_4As_4$ is not suppressed at all. Second, the T_{sc} values in $RbEu(Fe_{1-x}Ni_x)_4As_4$ are, on average, ~10 K lower than those in $Ba_{1-y}K_yFe_2As_2$ [52]. The amount of T_{sc} reduction is very close to that of Eu-free $Ba_{1-y}K_yFe_{1.86}Co_{0.14}As_2$ (compared in the same way to $Ba_{1-y}K_yFe_2As_2$) [47], suggesting that disorder plays the dominant role for suppression of T_{sc}. In other words, the Eu^{2+} spins play a relatively minor (if not none at all) role in suppressing SC. Third, the T_{sc} values of $RbEu(Fe_{1-x}Ni_x)_4As_4$ are even higher than those in Eu-diluted $Eu_{0.5}K_{0.5}(Fe_{1-x}Ni_x)_2As_2$ [48], the latter of which shows an antiferromagnetism (e.g., $T_N = 8.5$ K for $x = 0.08$) for

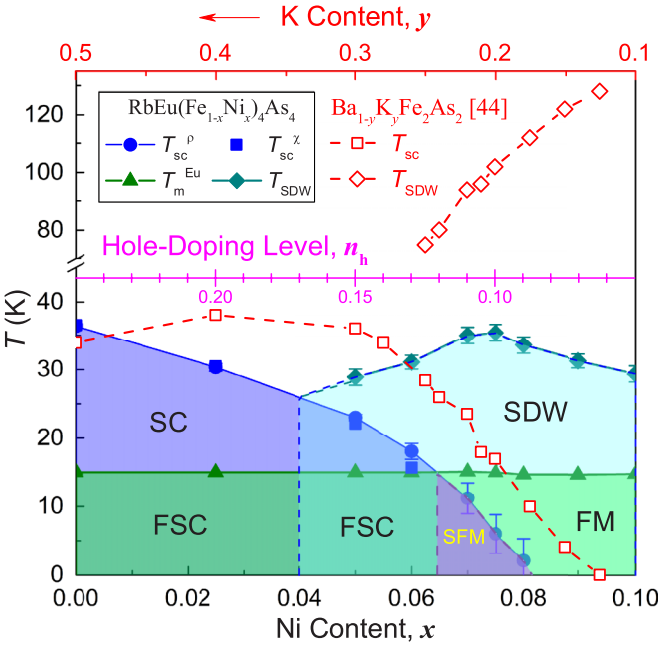

FIG. 8. Superconducting and magnetic phase diagram in RbEu(Fe$_{1-x}$Ni$_x$)$_4$As$_4$ containing various electronic phases highlighted with colors. T_{sc}^{ρ} is the midpoint temperature of superconducting resistive transitions, and the error bars denote the transition widths. T_{sc}^{χ} is the onset temperature of superconducting diamagnetic transitions. Other abbreviations include: SC, superconductivity; SDW, spin-density wave; FM, ferromagnet; FSC, ferromagnetic superconductor; SFM, superconducting ferromagnet. For comparison, the phase lines of Ba$_{1-y}$K$_y$Fe$_2$As$_2$ [52] are plotted using the top axis. Both horizontal axes share the same hole-doping level, $n_h = 0.25 - 2x = y/2$, as shown in the middle axis.

Eu^{2+} spins which implies relatively less influence on SC. This comparison further corroborates that Eu^{2+} spins hardly suppress T_{sc} in the 1144-type system.

In contrast to the dramatic changes in the states associated with the Fe sublattice, the ferromagnetic state in the Eu sublattice remains unchanged. In particular, T_m does not depend on the Ni doping, resulting in a crossing at $x \sim 0.065$ between the data lines of T_{sc} and T_m. According to the classification for materials with coexistence of SC and FM [5,9], the system changes from FSC to SFM at the crossing point. For $x > 0.08$, the system shows coexistence of Eu-spin FM and Fe-site SDW below 15 K. Although the sample with $x = 0.125$ (corresponding to $n_h = 0$) could not be synthesized owing to the solubility limit, one may expect by extrapolation that this completely hole-compensated material would show a similar behavior to that of the $x = 0.1$ sample.

F. Discussion

In the following, we discuss why both FSCs and SFMs exist in the RbEu(Fe$_{1-x}$Ni$_x$)$_4$As$_4$ system. First of all, the coexistence of SC and FM in Eu-containing 122-type iron pnictides was tentatively explained in terms of Fe-3d multi-orbitals and the robustness of SC [3]. On the one hand, multi-3d-orbitals in the valence band allow both SC mainly from $3d_{yz/zx}$ electrons and Eu-spin FM via Ruderman-Kittel-Kasuya-Yosida (RKKY) interactions through $3d_{x^2-y^2}$ and $3d_{z^2}$ electrons. On the other hand, the intrinsic upper critical field H_{c2}^* of the superconductors alike (e.g., an Eu-free analog) could be high enough to overcome the exchange field between Eu^{2+} spins and Cooper pairs.

In this context, the absence of SC for $T_{sc} < T_m$ in EuFe$_2$(As$_{1-x}$P$_x$)$_2$ [25,26], Eu(Fe$_{1-x}$Ni$_x$)$_2$As$_2$ [29], and Eu(Fe$_{1-x}$Co$_x$)$_2$As$_2$ [27] can be attributed to the relatively low H_{c2}^* in relation to the lower T_{sc}. Here we note that the Eu(Fe$_{0.81}$Co$_{0.19}$)$_2$As$_2$ single crystals grown from Sn flux were reported to show SC with $T_{sc} < T_m$ [45]. The possible reason is that the Eu-spin exchange field could be reduced due to the existence of defects in the Eu sublattice. One notes that the Sn-flux-grown "Eu(Fe$_{0.82}$Co$_{0.18}$)$_2$As$_2$" samples showed SDW order [53], indicating that they were actually in an underdoped regime. The underdoped status with heavy Co-doping levels suggests the possibility of significant Eu deficiencies. Besides, the flux Sn could also be incorporated into the Eu site [54]. Both factors lead to the dilution in the Eu sublattice, such that the exchange field that breaks Cooper pairs may be reduced, which helps the survival of SC.

In the 1144-type system of RbEu(Fe$_{1-x}$Ni$_x$)$_4$As$_4$, the Eu^{2+} spins hardly suppress SC. Therefore, not only do FSCs exist, but also SFMs occur in RbEu(Fe$_{1-x}$Ni$_x$)$_4$As$_4$. Note that the internal field generated from the Eu-spin FM is about 4.5 kOe, being high enough to induce spontaneous vortices, yet not high enough to destroy SC.

Finally, we comment on the magnetic interactions between Eu^{2+} spins in RbEu(Fe$_{1-x}$Ni$_x$)$_4$As$_4$. The experimental fact is that neither T_m nor Θ change with the Ni doping. This result contrasts to the change in T_m from 20 to 16 K, accompanying with an antiferromagnetic-to-ferromagnetic transition, only by 3% Ni doping in Eu(Fe$_{1-x}$Ni$_x$)$_2$As$_2$ [29]. The sensitivity to Ni doping dictates an indirect RKKY interaction whose strength is proportional to $\cos(2k_F r)/r^3$, where k_F is the Fermi vector and, r is the distance between Eu^{2+} spins. Conversely, the invariance of T_m and Θ against electron doping in RbEu(Fe$_{1-x}$Ni$_x$)$_4$As$_4$ suggests that the RKKY interaction may not be the dominant magnetic exchange interaction. This reminds us of the ferromagnetic europium chalcogenides, EuO ($T_m = 69.2$ K) and EuS ($T_m = 16.6$ K) [55], where there are no itinerant electrons for an indirect RKKY interaction. So the effective ferromagnetic couplings between Eu^{2+} spins in RbEu(Fe$_{1-x}$Ni$_x$)$_4$As$_4$ may be due to the so-called $d - f$ [56] and/or As $-$ Eu $-$ As superexchange interactions. Such exchange interactions naturally explain the decoupling between Eu-4f and Fe-3d orbitals, which conversely sheds light on the mechanism of iron-based superconductivity. Future theoretical analyses and calculations may help to clarify this issue.

IV. CONCLUSION

In summary, we systematically study the magnetic and superconducting properties in RbEu(Fe$_{1-x}$Ni$_x$)$_4$As$_4$ ($0 \leqslant x \leqslant 0.1$). With the Ni doping that introduces extra itinerant electrons, the self-doped holes are gradually compensated. As a result, the superconducting transition temperature T_{sc} decreases rapidly, and superconductivity disappears at $x \sim 0.08$. The hole depletion also brings the recovery of SDW order for $x \geqslant 0.05$. For the Eu sublattice, the Eu-spin ferromagnetism

in $RbEuFe_4As_4$ remains, and its Curie temperature keeps unchanged. This gives rise to unique SFMs showing absence of Meissner state. The realization of crossover from FSCs to SFMs makes $RbEu(Fe_{1-x}Ni_x)_4As_4$ a promising playground to look into the interplay between SC and FM for the future.

ACKNOWLEDGMENTS

This work was supported by the National Natural Science Foundation of China (No. 11474252) and National Key Research and Development Program of China (No. 2016YFA0300202).

Y.L. and Y.-B.L. contributed equally to this work.

[1] L. N. Bulaevskii, A. I. Buzdin, M. L. Kulić, and S. V. Panjukov, Coexistence of superconductivity and magnetism theoretical predictions and experimental results, Adv. Phys. **34**, 175 (1985).

[2] A. I. Buzdin, Proximity effects in superconductor-ferromagnet heterostructures, Rev. Mod. Phys. **77**, 935 (2005).

[3] G.-H. Cao, W.-H. Jiao, Y.-K. Luo, Z. Ren, S. Jiang, and Z.-A. Xu, Coexistence of superconductivity and ferromagnetism in iron pnictides, J. Phys.: Conf. Ser. **391**, 012123 (2012).

[4] E. B. Sonin and I. Felner, Spontaneous vortex phase in a superconducting weak ferromagnet, Phys. Rev. B **57**, R14000(R) (1998).

[5] B. Lorenz and C.-W. Chu, Superconducting ferromagnets: Ferromagnetic domains in the superconducting state, Nat. Mater. **4**, 516 (2005).

[6] Note that the terminology "ferromagnetic superconductor" is also occasionally employed in the literature related to the U-based germanides [7], which show $T_m > T_{sc}$.

[7] V. P. Mineev, Superconductivity in uranium ferromagnets, Physcis-Uspekhi **60**, 121 (2017).

[8] T. Nachtrab, C. Bernhard, C. Lin, D. Koelle, and R. Kleiner, The ruthenocuprates: natural superconductor-ferromagnet multilayers, C. R. Phys. **7**, 68 (2006).

[9] W.-H. Jiao, Q. Tao, Z. Ren, Y. Liu, and G.-H. Cao, Evidence of spontaneous vortex ground state in an iron-based ferromagnetic superconductor, Quant. Mater. **2**, 50 (2017).

[10] S. Zapf and M. Dressel, Europium-based iron pnictides: a unique laboratory for magnetism, superconductivity and structural effects, Rep. Prog. Phys. **80**, 016501 (2017).

[11] Z. Ren, Z. Zhu, S. Jiang, X. Xu, Q. Tao, C. Wang, C. Feng, G. Cao, and Z. Xu, Antiferromagnetic transition in $EuFe_2As_2$: A possible parent compound for superconductors, Phys. Rev. B **78**, 052501 (2008).

[12] S. Jiang, Y. Luo, Z. Ren, Z. Zhu, C. Wang, X. Xu, Q. Tao, G. Cao, and Z. Xu, Metamagnetic transition in $EuFe_2As_2$ single crystals, New J. Phys. **11**, 025007 (2009).

[13] J. Herrero-Martín, V. Scagnoli, C. Mazzoli, Y. Su, R. Mittal, Y. Xiao, T. Brueckel, N. Kumar, S. K. Dhar, A. Thamizhavel, and L. Paolasini, Magnetic structure of $EuFe_2As_2$ as determined by resonant x-ray scattering, Phys. Rev. B **80**, 134411 (2009).

[14] Y. Xiao, Y. Su, M. Meven, R. Mittal, C. M. N. Kumar, T. Chatterji, S. Price, J. Persson, N. Kumar, S. K. Dhar, A. Thamizhavel, and T. Brueckel, Magnetic structure of $EuFe_2As_2$ determined by single-crystal neutron diffraction, Phys. Rev. B **80**, 174424 (2009).

[15] Z. Ren, Q. Tao, S. Jiang, C. Feng, C. Wang, J. Dai, G. Cao, and Z. Xu, Superconductivity Induced by Phosphorus Doping and its Coexistence with Ferromagnetism in $EuFe_2(As_{0.7}P_{0.3})_2$, Phys. Rev. Lett. **102**, 137002 (2009).

[16] S. Jiang, H. Xing, G. Xuan, Z. Ren, C. Wang, Z.-a. Xu, and G. Cao, Superconductivity and local-moment magnetism in $Eu(Fe_{0.89}Co_{0.11})_2As_2$, Phys. Rev. B **80**, 184514 (2009).

[17] W.-H. Jiao, Q. Tao, J.-K. Bao, Y.-L. Sun, C.-M. Feng, Z.-A. Xu, I. Nowik, I. Felner, and G.-H. Cao, Anisotropic superconductivity in $Eu(Fe_{0.75}Ru_{0.25})_2As_2$ ferromagnetic superconductor, Europhys. Lett. **95**, 67007 (2011).

[18] W.-H. Jiao, H.-F. Zhai, J.-K. Bao, Y.-K. Luo, Q. Tao, C.-M. Feng, Z.-A. Xu, and G.-H. Cao, Anomalous critical fields and the absence of Meissner state in $Eu(Fe_{0.88}Ir_{0.12})_2As_2$ crystals, New J. Phys. **15**, 113002 (2013).

[19] U. B. Paramanik, D. Das, R. Prasad, and Z. Hossain, Reentrant superconductivity in $Eu(Fe_{1-x}Ir_x)_2As_2$, J. Phys.: Condens. Matter **25**, 265701 (2013).

[20] S. Nandi, W. T. Jin, Y. Xiao, Y. Su, S. Price, D. K. Shukla, J. Strempfer, H. S. Jeevan, P. Gegenwart, and T. Brückel, Coexistence of superconductivity and ferromagnetism in P-doped $EuFe_2As_2$, Phys. Rev. B **89**, 014512 (2014).

[21] S. Nandi, W. T. Jin, Y. Xiao, Y. Su, S. Price, W. Schmidt, K. Schmalzl, T. Chatterji, H. S. Jeevan, P. Gegenwart, and T. Brückel, Coexistence of ferromagnetism and superconductivity in iron based pnictides: a time resolved magnetooptical study, Phys. Rev. B **90**, 094407 (2014).

[22] W. T. Jin, S. Nandi, Y. Xiao, Y. Su, O. Zaharko, Z. Guguchia, Z. Bukowski, S. Price, W. H. Jiao, G. H. Cao, and T. Brückel, Magnetic structure of superconducting $Eu(Fe_{0.82}Co_{0.18})_2As_2$ as revealed by single-crystal neutron diffraction, Phys. Rev. B **88**, 214516 (2013).

[23] W. T. Jin, W. Li, Y. Su, S. Nandi, Y. Xiao, W. H. Jiao, M. Meven, A. P. Sazonov, E. Feng, Y. Chen, C. S. Ting, G. H. Cao, and T. Brückel, Magnetic ground state of superconducting $Eu(Fe_{0.88}Ir_{0.12})_2As_2$: A combined neutron diffraction and first-principles calculation study, Phys. Rev. B **91**, 064506 (2015).

[24] V. K. Anand, D. T. Adroja, A. Bhattacharyya, U. B. Paramanik, P. Manuel, A. D. Hillier, D. Khalyavin, and Z. Hossain, μSR and neutron diffraction investigations on the reentrant ferromagnetic superconductor $Eu(Fe_{0.86}Ir_{0.14})_2As_2$, Phys. Rev. B **91**, 094427 (2015).

[25] G. Cao, S. Xu, Z. Ren, S. Jiang, C. Feng, and Z. Xu, Superconductivity and ferromagnetism in $EuFe_2(As_{1-x}P_x)_2$, J. Phys.: Condens. Matter **23**, 464204 (2011).

[26] H. S. Jeevan, D. Kasinathan, H. Rosner, and P. Gegenwart, Interplay of antiferromagnetism, ferromagnetism, and superconductivity in $EuFe_2(As_{1-x}P_x)_2$ single crystals, Phys. Rev. B **83**, 054511 (2011).

[27] M. Nicklas, M. Kumar, E. Lengyel, W. Schnelle, and A. Leithe-Jasper, Competition of local-moment ferromagnetism and superconductivity in Co-substituted $EuFe_2As_2$, J. Phys.: Conf. Ser. **273**, 012101 (2011).

[28] R. Hu, S. L. Bud'ko, W. E. Straszheim, and P. C. Canfield, Phase diagram of superconductivity and antiferromagnetism in single crystals of $Sr(Fe_{1-x}Co_x)_2As_2$ and $Sr_{1-y}Eu_y(Fe_{0.88}Co_{0.12})_2As_2$, Phys. Rev. B **83**, 094520 (2011).

[29] Z. Ren, X. Lin, Q. Tao, S. Jiang, Z. Zhu, C. Wang, G. Cao, and Z. Xu, Suppression of spin-density-wave transition and emergence of ferromagnetic ordering of Eu^{2+} moments in $EuFe_{2-x}Ni_xAs_2$, Phys. Rev. B **79**, 094426 (2009).

[30] S. R. Saha, N. P. Butch, K. Kirshenbaum, and J. Paglione, Evolution of bulk superconductivity in $SrFe_2As_2$ with Ni substitution, Phys. Rev. B **79**, 224519 (2009).

[31] K. Kawashima, T. Kinjo, T. Nishio, S. Ishida, H. Fujihisa, Y. Gotoh, K. Kihou, H. Eisaki, Y. Yoshida, and A. Iyo, Superconductivity in Fe-based compound EuAFe$_4$As$_4$ (A = Rb and Cs), J. Phys. Soc. Jpn. **85**, 064710 (2016).

[32] Y. Liu, Y.-B. Liu, Z.-T. Tang, H. Jiang, Z.-C. Wang, A. Ablimit, W.-H. Jiao, Q. Tao, C.-M. Feng, Z.-A. Xu, and G.-H. Cao, Superconductivity and ferromagnetism in hole-doped $RbEuFe_4As_4$, Phys. Rev. B **93**, 214503 (2016).

[33] Y. Liu, Y.-B. Liu, Q. Chen, Z.-T. Tang, W.-H. Jiao, Q. Tao, Z.-A. Xu, and G.-H. Cao, A new ferromagnetic superconductor: $CsEuFe_4As_4$, Sci. Bull. **61**, 1213 (2016).

[34] H. Jiang, Y.-L. Sun, Z.-A. Xu, and G.-H. Cao, Crystal chemistry and structural design of iron-based superconductors, Chin. Phys. B **22**, 087410 (2013).

[35] A. Iyo, K. Kawashima, T. Kinjo, T. Nishio, S. Ishida, H. Fujihisa, Y. Gotoh, K. Kihou, H. Eisaki, and Y. Yoshida, New-structure-type Fe-based superconductors: $CaAFe_4As_4$ (A = K, Rb, Cs) and $SrAFe_4As_4$ (A = Rb, Cs), J. Am. Chem. Soc. **138**, 3410 (2016).

[36] G. Cao, S. Jiang, X. Lin, C. Wang, Y. Li, Z. Ren, Q. Tao, C. Feng, J. Dai, Z. Xu, and F.-C. Zhang, Narrow superconducting window in $LaFe_{1-x}Ni_xAsO$, Phys. Rev. B **79**, 174505 (2009).

[37] L. J. Li, Y. K. Luo, Q. B. Wang, H. Chen, Z. Ren, Q. Tao, Y. K. Li, X. Lin, M. He, Z. W. Zhu, G. H. Cao, and Z. A. Xu, Superconductivity induced by Ni doping in $BaFe_2As_2$ single crystals, New J. Phys. **11**, 025008 (2009).

[38] A. Arrott, Criterion for ferromagnetism from observations of magnetic isotherms, Phys. Rev. **108**, 1394 (1957).

[39] S. Zapf, H. S. Jeevan, T. Ivek, F. Pfister, F. Klingert, S. Jiang, D. Wu, P. Gegenwart, R. K. Kremer, and M. Dressel, $EuFe_2(As_{1-x}P_x)_2$: Reentrant Spin Glass and Superconductivity, Phys. Rev. Lett. **110**, 237002 (2013).

[40] P. W. Anderson and H. Suhl, Spin alignment in the superconducting state, Phys. Rev. **116**, 898 (1959).

[41] M. Fauré and A. I. Buzdin, Domain Structure in a Superconducting Ferromagnet, Phys. Rev. Lett. **94**, 187202 (2005).

[42] I. S. Veshchunov, L. Y. Vinnikov, V. S. Stolyarov, N. Zhou, Z. X. Shi, X. F. Xu, S. Y. Grebenchuk, D. S. Baranov, I. A. Golovchanskiy, S. Pyon, Y. Sun, W. Jiao, G. Cao, T. Tamegai, and A. A. Golubov, Visualization of the magnetic flux structure in phosphorus-doped $EuFe_2As_2$ single crystals, JETP Lett. **105**, 98 (2017).

[43] Note that the experimental value of M_{sat} increases further at lower temperatures and at higher magnetic fields.

[44] The internal magnetic field generated by Eu-spin ferromagnetism in $RbEuFe_4As_4$ is about a half of that (∼9 kOe) for an Eu-based 122-type compound [18,9] since the volume concentration of Eu moments of the former is only a half of that of the latter.

[45] V. H. Tran, T. A. Zaleski, Z. Bukowski, L. M. Tran, and A. J. Zaleski, Tuning superconductivity in $Eu(Fe_{0.81}Co_{0.19})_2As_2$ with magnetic fields, Phys. Rev. B **85**, 052502 (2012).

[46] H. Chen, Y. Ren, Y. Qiu, W. Bao, R. H. Liu, G. Wu, T. Wu, Y. L. Xie, X. F. Wang, Q. Huang, and X. H. Chen, Coexistence of the spin-density wave and superconductivity in $Ba_{1-x}K_xFe_2As_2$, Europhys. Lett. **85**, 17006 (2009).

[47] V. Zinth, T. Dellmann, H.-H. Klauss, and D. Johrendt, Recovery of a parentlike state in $Ba_{1-x}K_xFe_{1.86}Co_{0.14}As_2$, Angew. Chem. Inter. Ed. **50**, 7919 (2011).

[48] Anupam, V. K. Anand, P. L. Paulose, S. Ramakrishnan, C. Geibel, and Z. Hossain, Effect of Ni doping on magnetism and superconductivity in $Eu_{0.5}K_{0.5}Fe_2As_2$, Phys. Rev. B **85**, 144513 (2012).

[49] W. R. Meier, Q.-P. Ding, A. Kreyssig, S. L. Bud'ko, A. Sapkota, K. Kothapalli, V. Borisov, R. Valenti, C. D. Batista, P. P. Orth, R. M. Fernandes, A. I. Goldman, Y. Furukawa, A. E. Böhmer, and P. C. Canfield, Hedgehog spin vortex crystal in a hole-doped iron based superconductor, arxiv:1706.01067.

[50] F. Hardy, A. E. Böhmer, L. de' Medici, M. Capone, G. Giovannetti, R. Eder, L. Wang, M. He, T. Wolf, P. Schweiss, R. Heid, A. Herbig, P. Adelmann, R. A. Fisher, and C. Meingast, Strong correlations, strong coupling, and s-wave superconductivity in hole-doped $BaFe_2As_2$ single crystals, Phys. Rev. B **94**, 205113 (2016).

[51] L. Holmes and M. Schieber, Magnetic Ordering in Eu_3O_4 and $EuGd_2O_4$, J. Appl. Phys. **37**, 968 (1966).

[52] S. Avci, O. Chmaissem, D. Y. Chung, S. Rosenkranz, E. A. Goremychkin, J. P. Castellan, I. S. Todorov, J. A. Schlueter, H. Claus, A. Daoud-Aladine, D. D. Khalyavin, M. G. Kanatzidis, and R. Osborn, Phase diagram of $Ba_{1-x}K_xFe_2As_2$, Phys. Rev. B **85**, 184507 (2012).

[53] W. T. Jin, Y. Xiao, Z. Bukowski, Y. Su, S. Nandi, A. P. Sazonov, M. Meven, O. Zaharko, S. Demirdis, K. Nemkovski, K. Schmalzl, L. M. Tran, Z. Guguchia, E. Feng, Z. Fu, and T. Brückel, Phase diagram of Eu magnetic ordering in Sn-flux-grown $Eu(Fe_{1-x}Co_x)_2As_2$ single crystals, Phys. Rev. B **94**, 184513 (2016).

[54] Y. Su, P. Link, A. Schneidewind, T. Wolf, P. Adelmann, Y. Xiao, M. Meven, R. Mittal, M. Rotter, D. Johrendt, T. Brueckel, and M. Loewenhaupt, Antiferromagnetic ordering and structural phase transition in $Ba_2Fe_2As_2$ with Sn incorporated from the growth flux, Phys. Rev. B **79**, 064504 (2009).

[55] L. Passell, O. W. Dietrich, and J. Als-Nielsen, Neutron scattering from the Heisenberg ferromagnets EuO and EuS. I. The exchange interactions, Phys. Rev. B **14**, 4897 (1976).

[56] T. Kasuya, Exchange mechanisms in Europium chalcogenides, IBM J. Res. Dev. **14**, 214 (1970).